Supporting Information

Low-Temperature Purification of Phosphine (PH_3) Using CuO@NC Sorbents: Simultaneous Pollutant Removal and Cu_3P Resource Recovery

Zhongxian Wang§[a], Jiuyang He§[c], Jiayu Feng [d], Chaoyang Peng [b], Can Niu [e], Yixing Ma [a], Xin Sun [a], Fei Wang [a]*, Lian Wang [b]*, Ping Ning [a], Kai Li [a]*

Affiliations:

a Faculty of Environmental Science and Engineering, Kunming University of Science and Technology, Kunming 650500, China.

b Laboratory of Atmospheric Environment and Pollution Control, Research Center for Eco-Environmental Sciences, Chinese Academy of Sciences, Beijing 100085, China

c Experimental Center of Advanced Materials, School of Materials Science & Engineering, Beijing Institute of Technology, Beijing 100081, China

d School of Chemistry and Environment, Yunnan Minzu University, Kunming, Yunnan 650504, China

e Key Laboratory of Public Health Safety of Hebei Province, College of Public Health, Hebei University, Baoding, 071002, China

* **Corresponding author:**

Fei Wang – *Faculty of Environmental Science and Engineering, Kunming University of Science and Technology, Kunming 650500, China; National-Regional Engineering Center for Recovery of Waste Gases from Metallurgical and Chemical Industries, Kunming 650500, China*

Email: wangfei@kust.edu.cn

Lian Wang – *Laboratory of Atmospheric Environment and Pollution Control, Research Center for Eco-Environmental Sciences, Chinese Academy of Sciences, Beijing 100085, China*

Email: lianwang@rcees.ac.cn

Kai Li – *Faculty of Environmental Science and Engineering, Kunming University of Science and Technology, Kunming 650500, China; National-Regional Engineering Center for Recovery of Waste Gases from Metallurgical and Chemical Industries, Kunming 650500, China*

Email: kli@kust.edu.cn

Summary of Contents:

Pages: 34

Appendix: 5

Figures: 18

Tables: 5

Table of contents

Appendix S1: Preparation of sorbents

Materials. Copper nitrate ($Cu(NO_3)_2 \cdot 3H_2O$, 99%) and urea (CH_4N_2O, 99%) were purchased from Aladdin Co. Ltd (Shanghai, China) and used as supplied. The PH_3 gas was purchased from Dalian special gases Co. Ltd. O_2 and N_2 were obtained from Kunming Guangruida special Gases Co. Ltd.

Synthesis of the CuO@NC-doped sorbents. The typical synthesis of CuO@NC-doped sorbents is as follows: $Cu(NO_3)_2 \cdot 3H_2O$ was mixed with CH_4N_2O together. Then, the obtained precursors were calcined in a tube furnace at 550℃ (ramp rate: 3℃/min) for 3 h under an air atmosphere. The sorbent was designed as CuO@NC. The comparison samples were similarly synthesized except for the different content of $Cu(NO_3)_2 \cdot 3H_2O$ in the raw materials, and they are named 1CuO@NC, 2CuO@NC, 3CuO@NC, 4CuO@NC, and CuO particles according to the mass ratio of $Cu(NO_3)_2 \cdot 3H_2O$: CH_4N_2O (1:6, 2:6, 3:6, 4:6, and 4:0), respectively.

Appendix S2: Characterization methods

The specific surface area was calculated using the Brunauer−Emmett−Teller (BET) method using a surface area analyzer (BELSORP-max, MicrotracBEL, Japan) at the temperature of liquid nitrogen (77 K). Before the analysis, all samples were degassed at 473 K for 3 h. The BET surface area, total pore volume, and pore size distribution were calculated using adsorption/desorption isotherms. Horvath-Kawazoe (HK) method and Barrett-Joyner-Halenda (BJH) method were used to calculate the pore size distribution, the total pore volume (V_{total}), and the mesopore volume (V_{mes}), and the micropore volume (V_{mic}) of the sorbents. The reaction process was investigated by in situ IR spectroscopy using an infrared spectrophotometer (Thermo Scientific Nicolet Is 50, USA). The sample (~0.05 g) was placed into a pot with a diluted amount of reactant and with a heating cartridge that allowed the samples to be heated to the desired temperature (~80℃). All the spectra acquired were accumulated over 16 scans performed with a resolution of 4 cm^{-1}. The x-ray diffraction (XRD) patterns were obtained using an X-ray diffractometer (Rigaku Miniflex 600) equipped with Ni-filtered Cu Ka radiation(λ=0.15406 nm) opening at a scan rate of 5° min^{-1} from 2ϑ = 10–90°. The identification of the crystalline phases was performed by matching the samples with JCPDS files, and the crystallinity was calculated using MDI Jade 6.0. The X-ray Photoelectron Spectroscopy (XPS) (K-alpha+, Thermo Fisher Scientific) analysis was performed using Al Kα radiation, where the energy of the Al target power was at 72 W. The Fourier transform infrared (FT-IR) analysis was carried out using an infrared spectrophotometer (Thermo Scientific Nicolet Is 50, USA). The instrument was scanned 32 times over a test range of 400–4000 cm^{-1}, and the resolution of the instrument was 4 cm^{-1}. Thermogravimetric (TG-DTG) curves were carried out on a METTLER TOLEDO TGA analyzer. The uncalcined precursor was heated up to temperatures of 800 °C at a heating rate of 5℃ min^{-1} with an N_2 flow. Raman spectra were collected on a Renishaw inVia instrument confocal Raman microscope using a 633 nm laser at 5 mW, and a 50x objective, by accumulating 5 scans, with an integration time of 10 s. The surface morphologies and microstructures of the samples were observed with scanning electron microscopy (SEM) (Zeiss Gemini 300) equipped with an EDS system, operating at 3.00 kV. The morphology and structure of the materials were characterized by a transmission electron microscope (JEM-2100 plus, JEOL, Japan) operated at an accelerating voltage of 200 kV.

Moreover, the hydrogen temperature-programmed reduction (H_2-TPR) experiments were performed using AutoChem1 II 2920 equipment under the conditions of 10 vol% H_2/Ar flow, and 10°C•min^{-1}. Electron paramagnetic resonance (EPR) spectra were recorded on an EMXmicro (Burker, Germany) spectrometer at ambient temperature. The photoelectrochemical (PEC) measurements were performed on a CHI 660E electrochemical workstation (CHI Inc., USA) at ambient temperature. Transient photocurrents measurement was recorded under intermittently visible light irradiation (λ > 420 nm). Photoluminescence (PL) experiments were tested by a transient fluorescence spectrophotometer (Edinburgh Instruments, EI, FLS1000). Cu_3P was dispersed into varying concentrations within deionized water and subjected to mechanical stirring at a temperature of 25°C to ensure a homogeneous suspension. At predetermined time intervals of 10 minutes and 30 minutes post-dispersion, a 1 mL aliquot of the suspension was extracted and centrifuged to separate the solid nanoparticles from the supernatant. The supernatant was then analyzed for the dissolution of Cu^{2+} using a PerkinElmer Optima 8300 Inductively Coupled Plasma Optical Emission Spectrometer (ICP-OES). The PerkinElmer Optima 8300 ICP-OES is a state-of-the-art analytical instrument designed for the simultaneous determination of multiple elements.

Appendix S3: Experimental setup

The sorbents performance test system is shown in Fig. S1. The tests for sorbent performance were carried out in a custom quartz tube fixed-bed reactor (135 mm length × 6 mm insider diameter). Before evaluating the PH_3 removal performance of the sorbents, a pre-cleaning with N_2 was performed at 100°C for 30 min to remove the adsorbed water from the surface of the sorbents. PH_3 from the gas cylinder was diluted with N_2 (99.99%) to the required concentrations (1% O_2, *C (PH₃)*: 1000 ppm/1517.86 mg m^{-3}, ±5%), which is a typical O_2 and PH_3 concentration measured in the yellow phosphorus tail gas. In this study, the total flow rate (*Q*) and the mass of sorbent were fixed at 100 mL $min^{-1}$and 0.3 g, which corresponded to a weight hourly space velocity (*WHSV*) of 20 000 mL $h^{-1}g_{sorbent}^{-1}$. Use an electric tracing ribbon to keep the reactor temperature (*T*) at 90°C. The PH_3 concentrations in the inlet and outlet gases of the reactor were determined using an online 9790 Ⅱ gas chromatograph. The PH_3 concentration was measured every 20 min until the PH_3 concentration in the outlet gas reached 30 ppm. Experiments on each sorbent were repeated twice to assess the reliability of the data collected. The removal efficiency and PH_3 breakthrough capacity are defined in Equations 1 and 2, respectively. Note that the breakthrough capacity is defined as when the removal efficiency is 97%.

$$PH_3 \text{ removal efficiency (\%)} = \frac{C_{inlet} - C_{outlet}}{C_{inlet}} \times 100 \quad (1)$$

$$PH_3 \text{ breakthrough capacity (mg}(PH_3)\ g_{sorbent}^{-1}) = \frac{Q\int_0^t (C_{inlet} - C_{outlet})dt}{m} \quad (2)$$

Where C_{inlet} and C_{outlet} are the PH_3 concentration in the inlet gas and outlet gas (mg m^{-3}), *m* is the mass of fresh sorbents (0.3 g), and *t* is the reaction time (min), and *Q* is the total flow rate (100 mL min^{-1}).

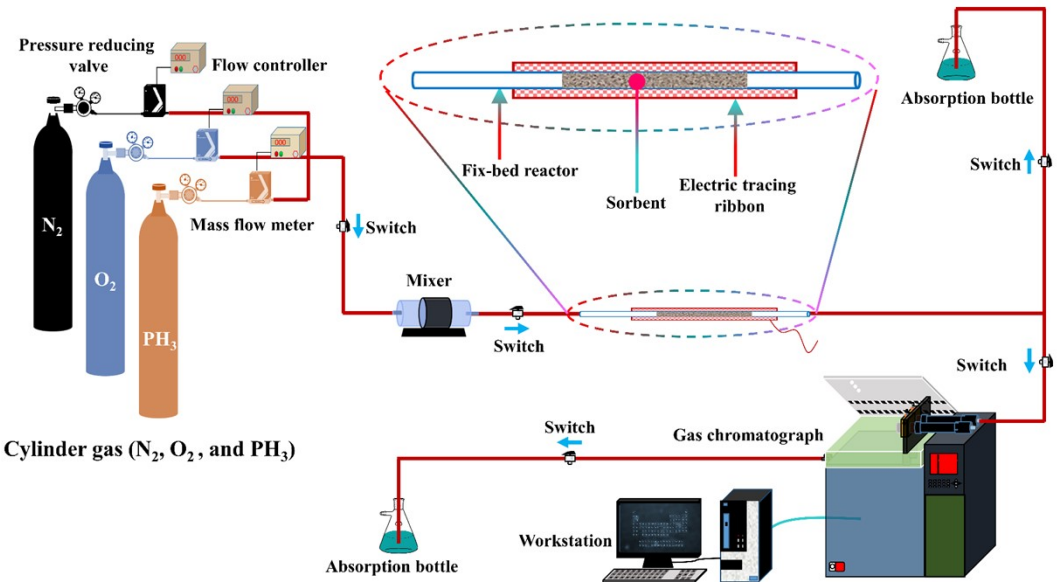

156

157 **Scheme S1.** Adsorption–oxidation performance test system.

158

Appendix S4: Photocatalytic performance measurement

Photocatalytic removal of Hg^0

The simulated gas was first mixed with ~2% O_2 and 1100 ± 100 μg m^{-3} Hg^0(gas) (N_2 balance) and then introduced into a fixed bed reactor. The photocatalytic removal efficiency of Hg^0(gas) was evaluated at room temperature, in which each group of 50 mg catalyst was added into a quartz tube exposed to 1100 ± 100 μg m^{-3} Hg^0(gas) (N_2 balance) at the flow intake rate of 400 mL min^{-1} (GHSV=480 000 mL $h^{-1}g_{catalyst}^{-1}$). During adsorption, the catalyst was irradiated with UV light (254 nm, 3 mW cm^{-2}, Philips) and then swept with He gas at 50℃ for 30 min to remove the physically adsorbed oxygen. Adsorption saturation was achieved when the light was turned off. The experiment was then initiated and stopped when the reaction removal efficiency reached saturation. The concentration of Hg^0(gas) was measured using a QM201 fluorescent mercury meter, and the final removal efficiency was calculated by using the following formula:

$$Hg^0(gas)\ \text{removal efficiency}\ (\%) = \frac{C_{inlet} - C_{outlet}}{C_{inlet}} \times 100$$

where C_{inlet} and C_{outlet} are the Hg^0(gas) concentrations in the inlet gas and outlet gas (μg m^{-3}), respectively, and Q is the total flow rate (400 mL min^{-1}).

Photocatalytic degradation of Rhodamine B (RhB)

First, 50 mg catalyst was added to 50 mL rhodamine B (RhB) solution at a concentration of 40 mg/L and magnetically stirred for 60 min under dark conditions to achieve adsorption and desorption equilibrium. Next, a 500 W xenon lamp with a 420 nm cut-off filter was used as the visible light source, and a circulating cooling system was used to control the reaction temperature at 25℃. During the photocatalytic reaction, 3 mL of the suspension was collected every 15 min and centrifuged at 5000 rpm for 3 min to obtain the supernatant. The photocatalytic degradation efficiency of RhB was measured at 554 nm using a UV-vis spectrophotometer.

Appendix S5: Bactericidal activity testing

E. coli inactivation assay

Single colonies of *E. coli* (ATCC 25922) cultured on LB solid medium were selected and incubated at 37 °C in LB liquid medium for 12 h, then centrifuged and washed twice to collect *E. coli*, which was then dispersed into deionized water to obtain about 10^8 CFU/mL *E. coli*. Next, the De-2CuO@NC powder with different quality was added into *E. coli* suspension to form various concentration of De-2CuO@NC (5,10,15 mg·L^{-1}). The mixture was stirred with a magnetic stirrer at 25 °C. At the time intervals of 10 min and 30 min after De-2CuO@NC addition, 0.5 mL of bacterial suspension was withdrawn and immediately diluted 10-fold in series with 4.5 mL deionized water and plated on LB agar plates. All plates were cultured at 37 ℃ for 12 h and viable cell counts were determined using standard plate counting method. All experiments were repeated in triplicate.

H1N1 Influenza virus inactivation experiment

The effect of De-2CuO@NC on virus was examined at GUANGDONG DETECTION CENTER OF MICROBIOLOGY, China. First, the virus suspension (Influenza A virus, H1N1 A/PR/8/34, ATCC CR-1469) was added to cell culture plate to infect MDCK cell. The cell suspension was added to the wells of a 96-well plate and cultured for 24 h (5% CO_2, 37 ℃) for complete attachment, followed by the virus suspension added and laid aside at 37 ℃ for 1-2 h. Subsequently, after removing the original culture medium and rinsing with PBS three times, culture was conducted in 5% CO_2 atmosphere at 37 ℃ for 1 h. Finally, the virus suspension in the cell culture plate was removed. After culturing for another 24 h, the virus infection of MDCK cells was observed and recorded by using an inverted fluorescence microscope. 100 μL of virus stock solution was dropped into the De-2CuO@NC suspension (15 mg·L^{-1}), then shaked in a shaker for 30 min, followed by virus titer test ($TCID_{50}$ method) and incubated in 5% CO_2 atmosphere at 34 ℃ for 7 days. Finally, cell lesions were observed and virus titers were calculated. Deionized water was used for positive control. Cell culture medium was used as a negative control, confirming the culture medium used was not contaminated and the cells were growing well.

The oxidation performance of De-2CuO@NC

In order to examine the oxidation performance of De-2CuO@NC such as lipid peroxidation towards *E. coli* cells, the concentration of malondialdehyde (MDA) in *E. coli* suspension treated with De-2CuO@NC for 30 min was tested with Tongren chemical kit.

Cytotoxicity assays

De-2CuO@NC was dispersed into suspension using sterilized deionized water, and Hela cells were cultured in Dulbecco's Modified Eagle Medium (DMEM) media overnight in 96-well plates. The culture media was removed and washed twice with PBS. The final ratio of DMEM media and suspension was 9:1（15 $mg \cdot L^{-1}$), the mixture was added to 96-well plate and incubated for 24 h, the media was removed and washed twice with PBS, and the Cell Counting Kit-8 (CCK8) and DMEM media were mixed at the ratio of 1:9 and incubated for 2 h, and the absorbance was detected at 405 nm wavelength on a microplate reader.

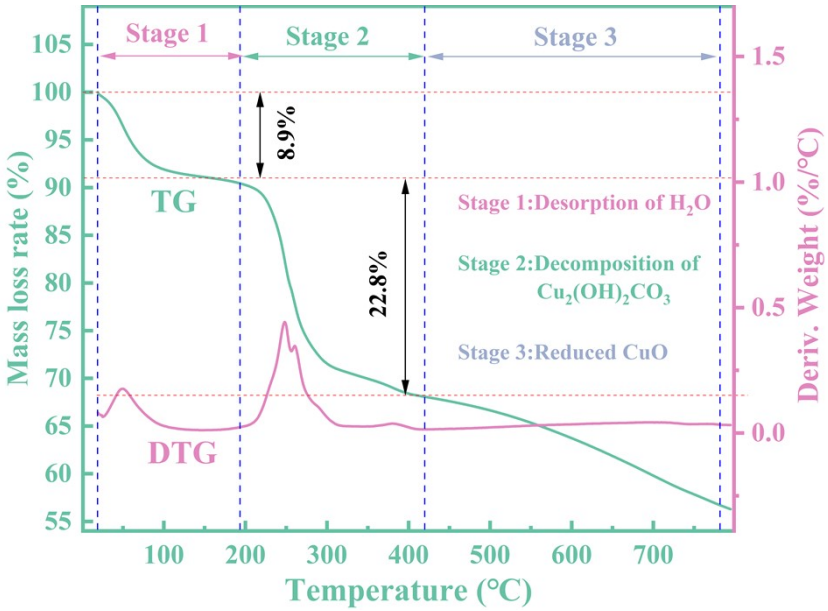

Figure S1. Thermogravimetric (TG) and derivative thermogravimetric (DTG) curves of 2CuO@CN.

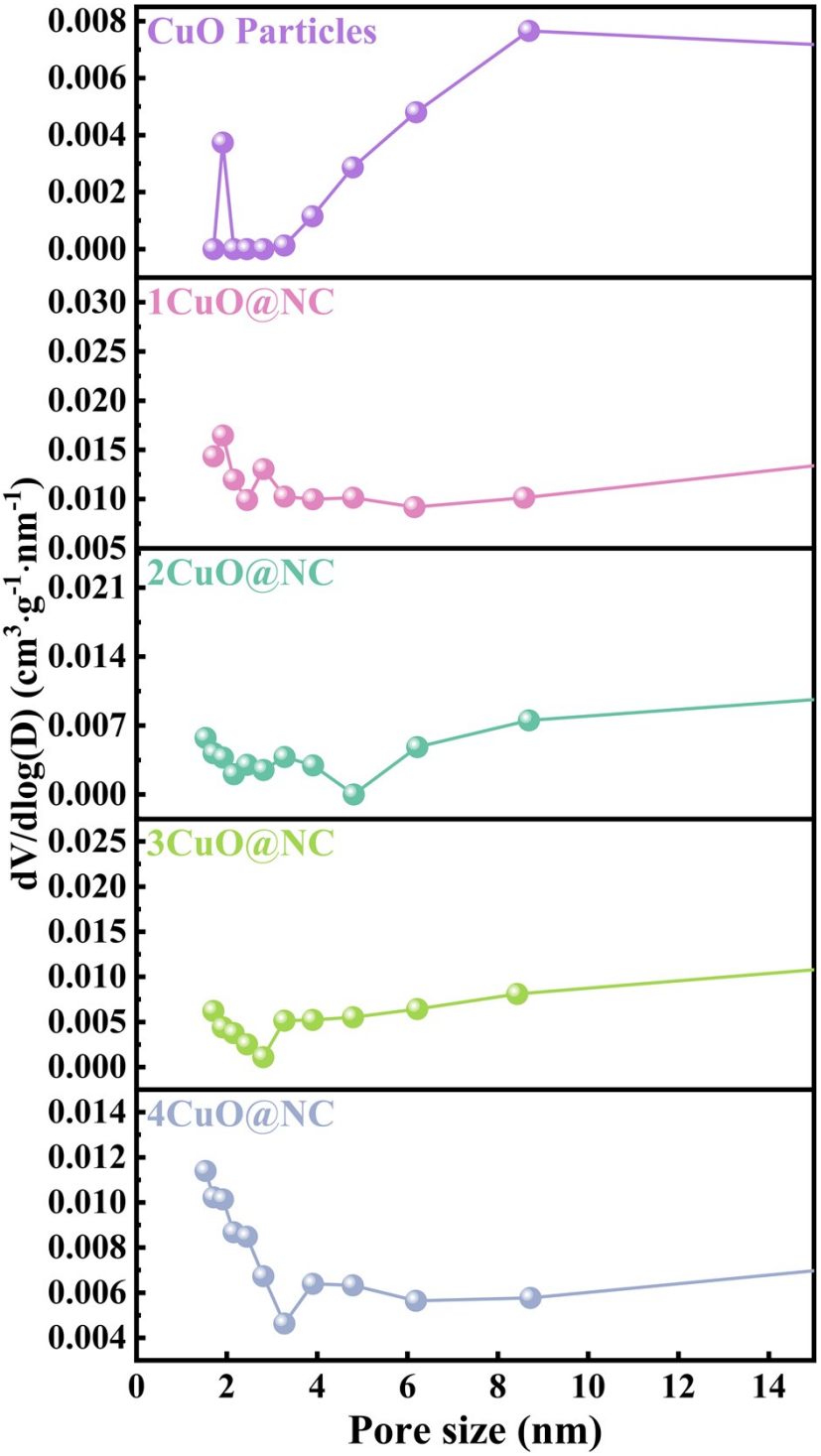

Figure S2. BJH pore size distribution of the material.

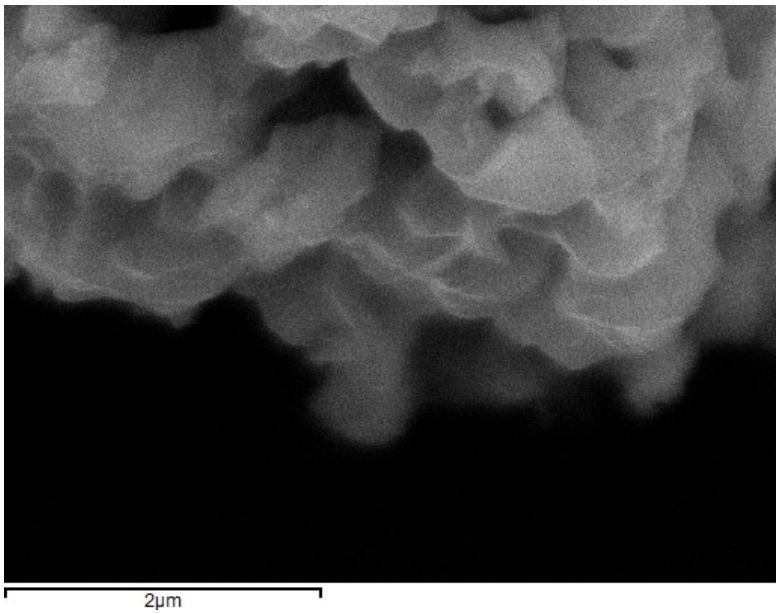

Figure S3. SEM micrographs of the 2CuO@CN.

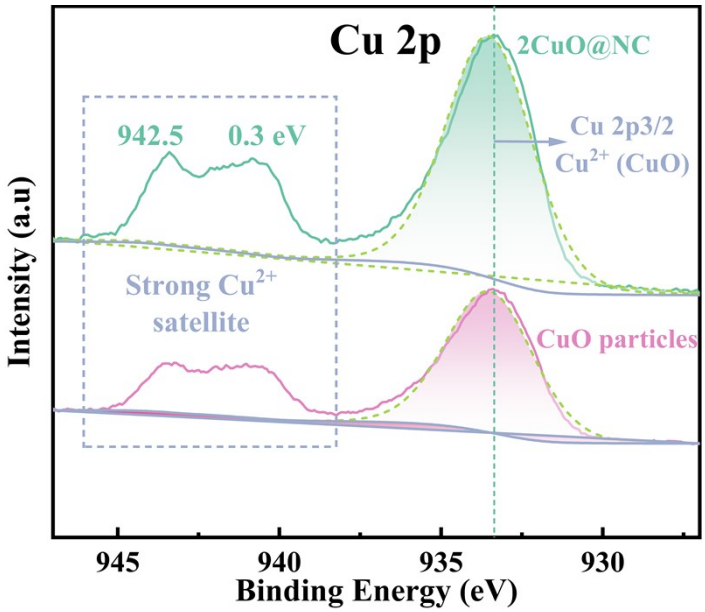

Figure S4. Cu $2p_{3/2}$ photoelectron spectra of CuO particles and 2CuO@NC.

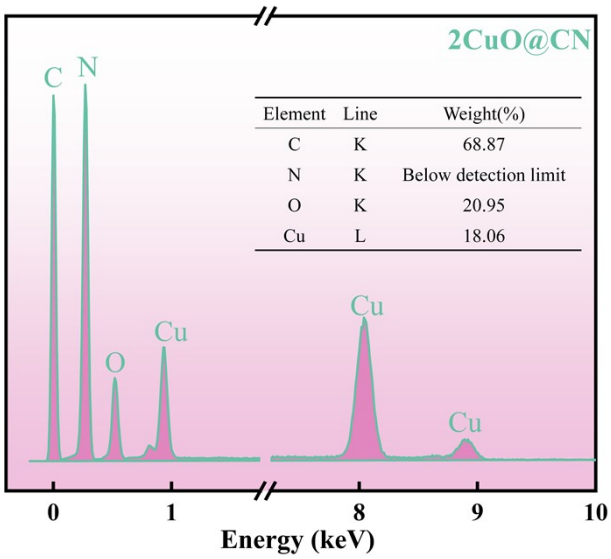

Figure S5. EDS element analysis of 2CuO@CN.

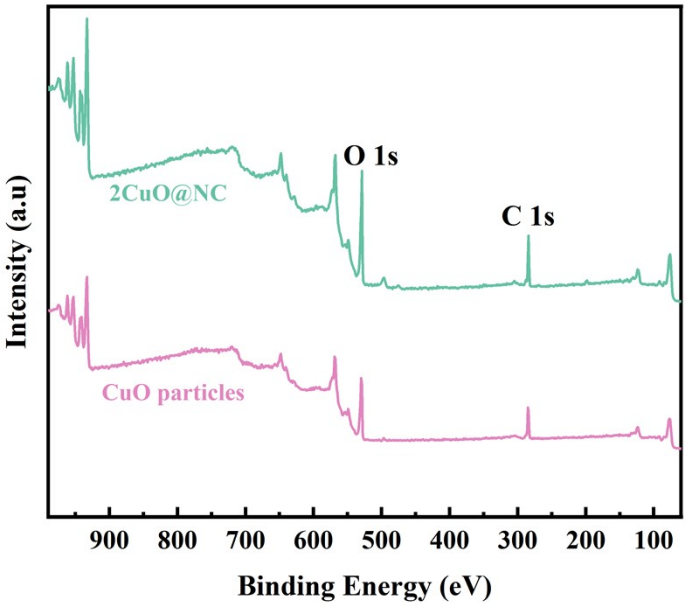

239

240 **Figure S6.** Wide-survey XPS spectra of CuO particles and 2CuO@NC.

241

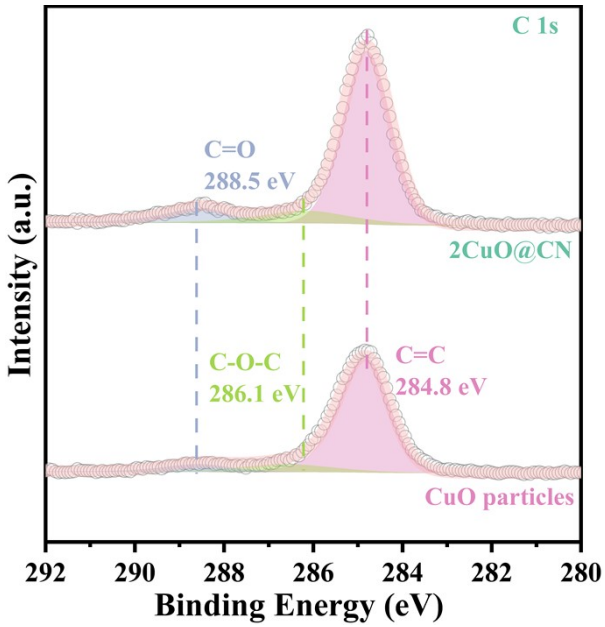

242

243 **Figure S7.** C 1s spectra of CuO particles, and 2CuO@NC

244

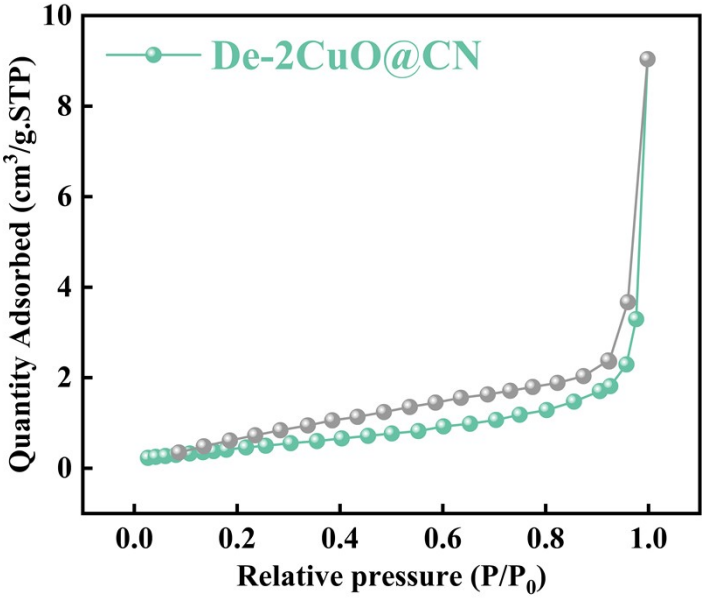

Figure S8. N_2 adsorption/desorption isotherms of De-2CuO@CN. The desorption curve is shown as a gray line.

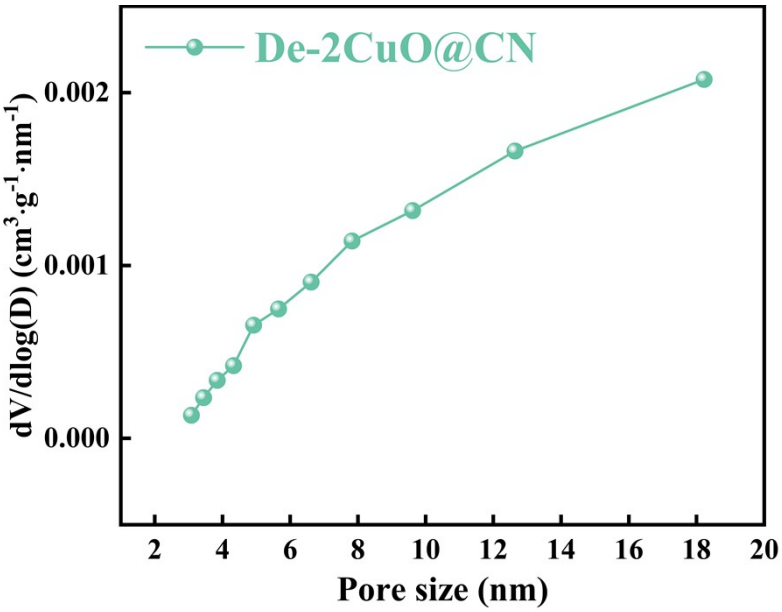

Figure S9. BJH pore size distribution of De-2CuO@CN.

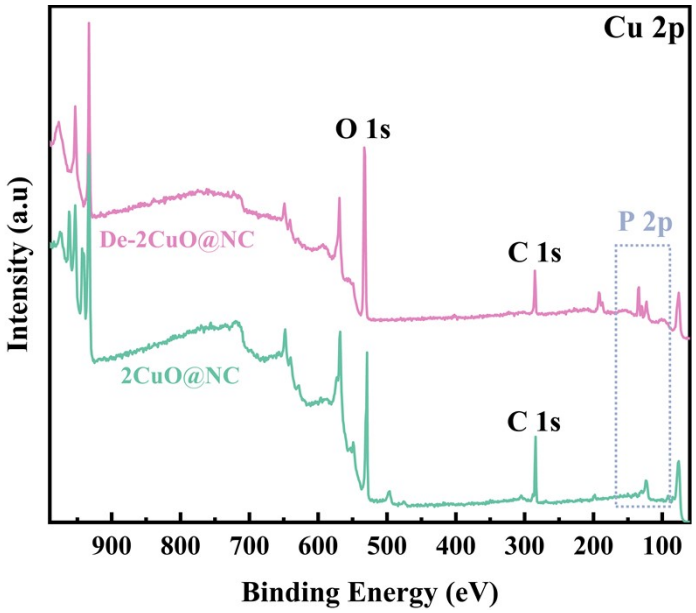

252

253 **Figure S10**. Wide-survey XPS spectra of 2CuO@NC and De-2CuO@NC.

254

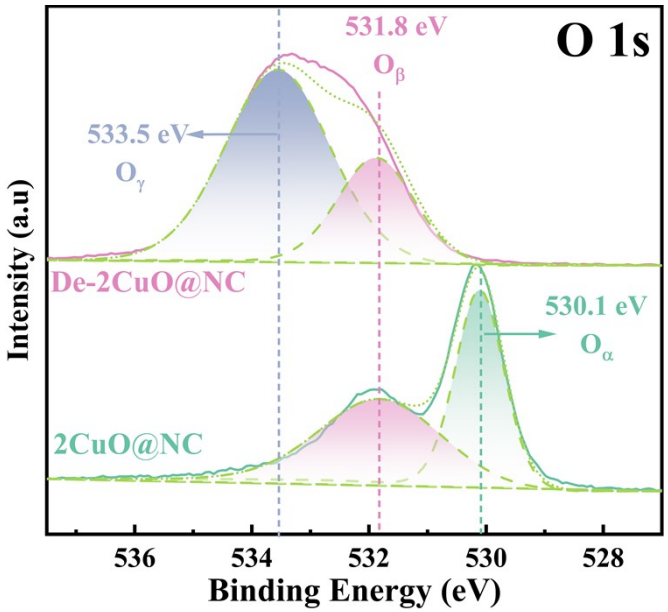

255

256 **Figure S11.** O 1s photoelectron spectra of 2CuO@NC and De-2CuO@NC.

257

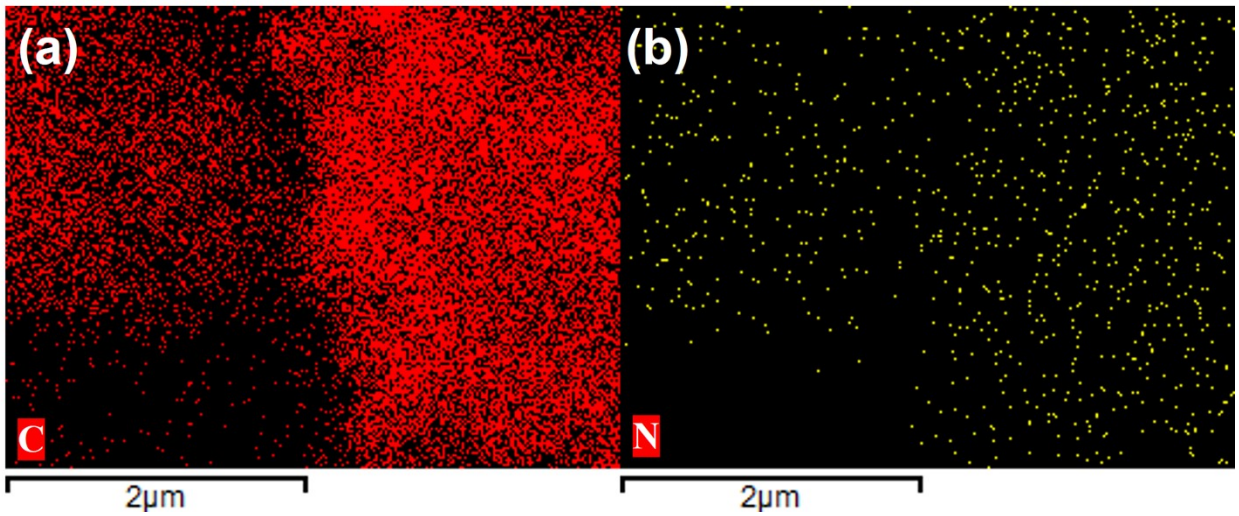

Figure S12. EDS mapping image of the elemental distribution of (a) C and (b) N.

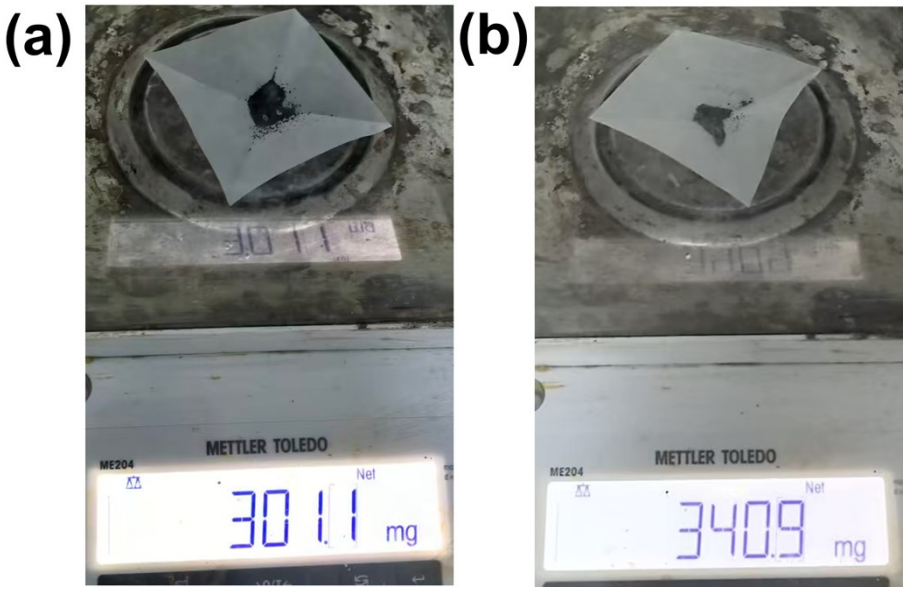

Figure S13. Mass of the adsorbent (a) before and (b) after adsorption.

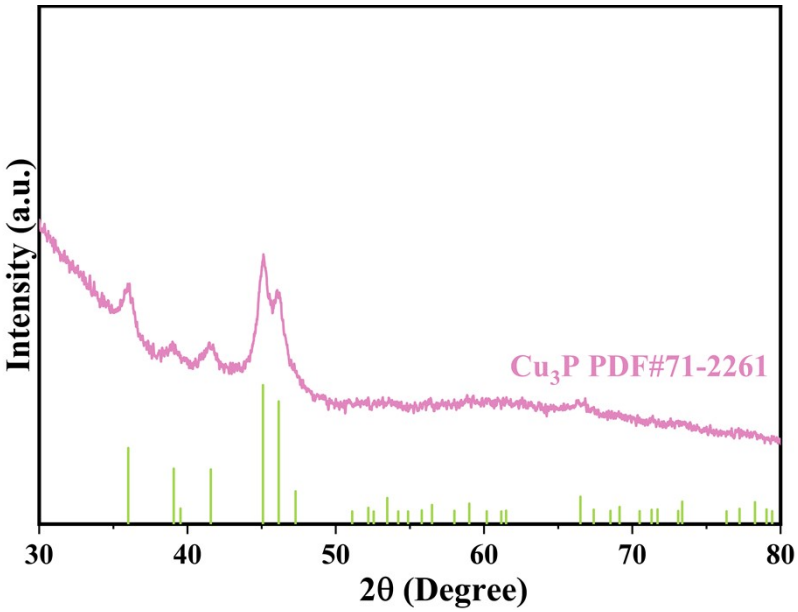

Figure S14. XRD patterns of De-2CuO@CN after RhB photocatalytic degradation.

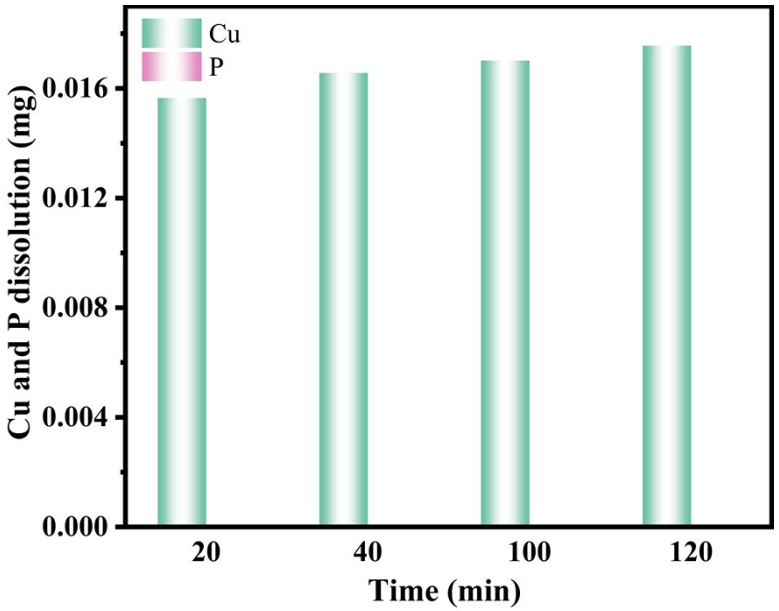

Figure S15. Elemental leaching amounts of Cu and P from De-2CuO@CN after RhB photocatalytic degradation measured by ICP analysis.

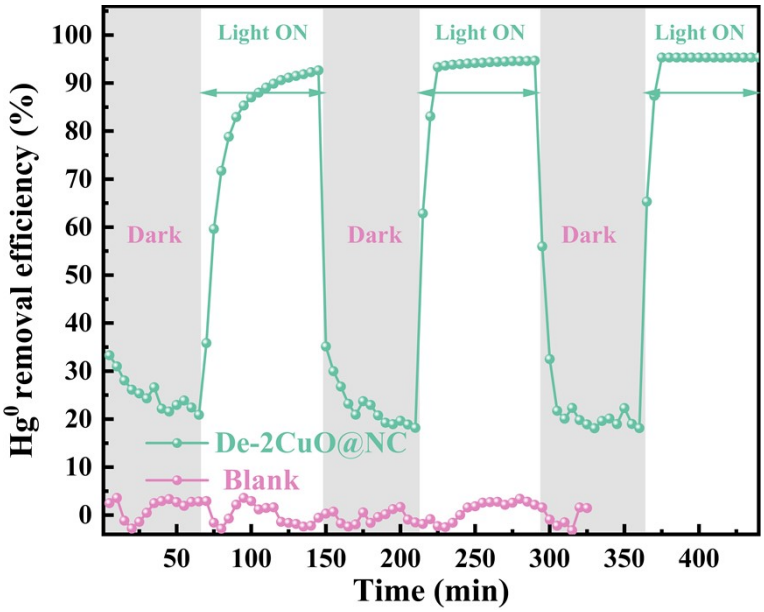

Figure S16. Photocatalytic removal of Hg^0 (gas) under UV light (254 nm) irradiation of De-2CuO@NC

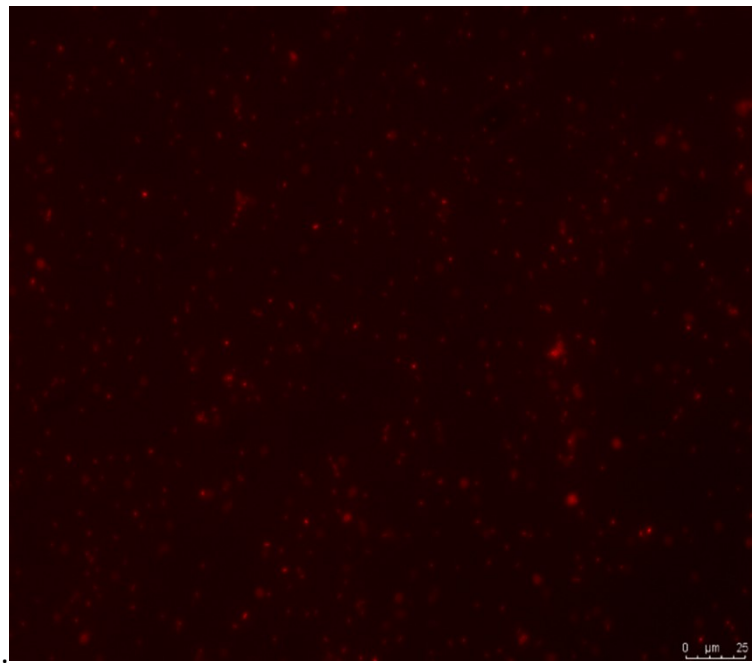

Figure S17. Photographs of fluorescence microscope of *E. coli* treated with mg·L^{-1} De-2CuO@NC samples for 30 min after stained with 3 µM propidium iodide (PI); Initial bacterial concentration 1×10^{8} CFU/mL.

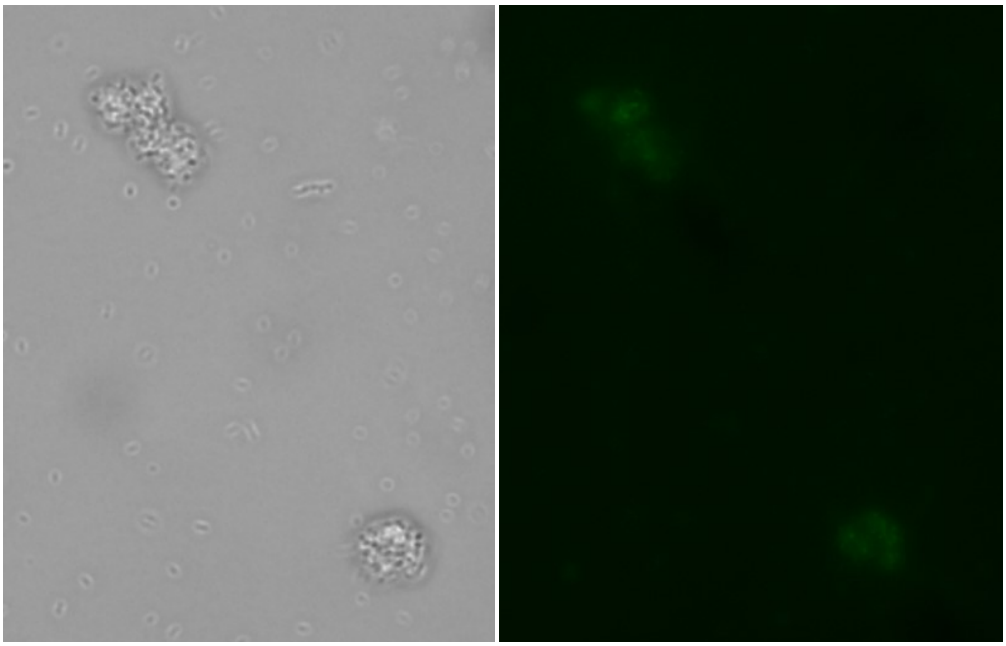

Figure S18. Photographs of fluorescence microscope of *E. coli* treated with 15 mg·L^{-1} De-2CuO@NC samples for 30 min after stained with 10 μM DCFH-DA. Initial bacterial concentration 1×10^8 CFU/mL.

285 **Table S1.** Physical properties of the various samples.

Sample	S (m^2 g^{-1})	V_{total} (cm^3 g^{-1})	D (nm)
CuO	0.95	0.01	12.3
1CuO@NC	9.7	0.04	8.1
2CuO@NC	7.1	0.03	7.5
3CuO@NC	6.3	0.03	9.6
4CuO@NC	5.6	0.02	7.2

286

287 **Table S2.** Physical properties of De-2CuO@CN.

Sample	S (m^2 g^{-1})	V_{total} (cm^3 g^{-1})	D (nm)
De-2CuO@NC	1.94	0.014	3.1

288

289

Table S3. Summary of photocatalyst performance in some literature reports for photocatalytic degradation of RhB.

Catalyst	Light	Concentration	Solution volume	Performance	Ref.
TiO_2/MMT	Sunlight	10 ppm	100 mL	200 min 90%	[1]
graphene–ZnO	Sunlight	10 mg/L	100 mL	140min 100%	[2]
MCM-glypy-Mo	Visible light	20 ppm	150 mL	120min 100%	[3]
TiO_2nanotubes	Visible light	16 mg·L^{-1}	200 mL	140 min 94.86%	[4]
Anatase TiO_2 Nanowires	UV light	23 mg·L^{-1}	10 mL	50 min 100%	[5]
MoP QDs (PMO-5)	Visible light	50 mg/L	50 mL	40 min 97%	[6]
P-doped porous g-C_3N_4	Visible light	20 mg/L	200 mL	70 min 99.5%	[7]
Ag_3PO_4/NG/P_3HT	Visible light	10 mg/L	50 mL	32 min 95%	[8]
Ag_3PO_4	Visible light	20 mg/L	200 mL	21 min 95%	[9]
De-2CuO@NC	**Visible light**	**50** mg·L^{-1}	**50 mL**	**120 min 100%**	**This work**

Table S4. XPS elemental composition of 2CuO@CN.

Name	Area	Atomic (%)
C1s	56512.99	32.95
Cu2p	670763.72	26.25
O1s	155021.94	37.33
N1s	2535.67	0.96

Table S5. H1N1 influenza virus inactivation assay results

Virus and host cell	Action concentration and time	Group	Logarithm of infectivity titre value ($lgTCID_{50}$/mL)	Average logarithm of infectivity titre value ($lgTCID_{50}$/mL)	Infectivity titre virus value(TCD_{50}/mL)	Average infectivity titre virus value(TCD_{50}/mL)	Virus inactivation ratio(%)
Influenza A virusHIN1:AVPR/8/34 (ATCC VR-1469) Host cell: MDCK	15 $mg·L^{-1}$ 30 min	Control group 1	5.43	5.42	$2.66*10^5$	1.03	90.68
		Control group 2	5.50				
		Control group 3	5.33				
		Test group 1	4.33				
		Test group 2	4.50	4.39	$2.48*10^4$		
		Test group 2	4.33				
Cells in the negative control group grew well, the results met all the requirements of the evaluation criteria.							

REFERENCE

[1] T.B.T. Dao, T.T.L. Ha, T.D. Nguyen, H.N. Le, C.N. Ha-Thuc, T.M.L. Nguyen, P. Perre, D.M. Nguyen, *Chemosphere* 2021, **280**, 130802.

[2] G.M. Neelgund, A. Oki, Z. Luo, *J. Colloid Interface Sci.* 2014, **430**, 257-264.

[3] N.U. Silva, T.G. Nunes, M.S. Saraiva, M.S. Shalamzari, P.D. Vaz, O.C. Monteiro, C.D. Nunes, *Appl. Catal. B Environ.* 2012, **113**: 180-191.

[4] Y.L. Pang, A.Z. Abdullah, S. Bhatia, , *Chem. Eng. J.* 2011, **166**, 873-880.

[5] H.B. Wu, H.H. Hng, X.W. Lou, *Adv. Mater.*, 2012, **24**, 2567-2571.

[6] Y. Huang, W. Xing, L. Zhou, B. Tian, J. Zhang, Y. Zhou, *Res. Chem. Intermed.* 2022, **48**, 2887.

[7] Z. Li, Q. Chen, Q. Lin, Y. Chen, X. Liao, H. Yu, C. Yu, *J. Taiwan Inst. Chem. Eng.* 2020, **114**, 249.

[8] Y. Zhang, C. Xie, F. L. Gu, H. Wu, Q. Guo, *J. Hazard. Mater.* 2016, **315**, 23.

[9] J. Ma, Q. Liu, L. Zhu, J. Zou, K. Wang, M. Yang, S. Komarneni, *Appl. Catal. B: Environ.* 2016, **182**, 26.